Accepted Manuscript
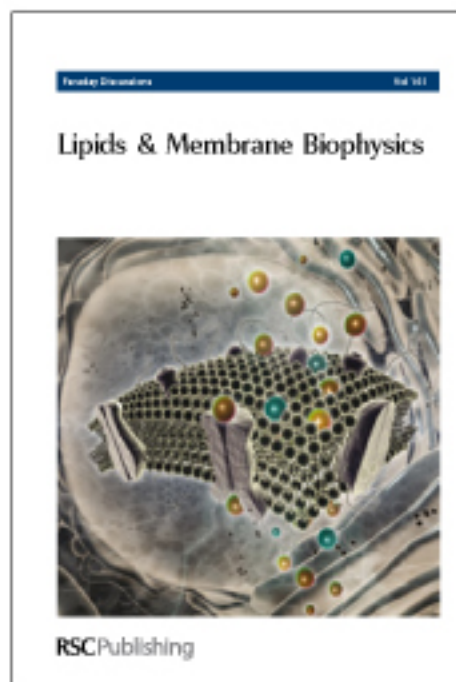
This is an *Accepted Manuscript*, which has been through the RSC Publishing peer review process and has been accepted for publication.

Accepted Manuscripts are published online shortly after acceptance, which is prior to technical editing, formatting and proof reading. This free service from RSC Publishing allows authors to make their results available to the community, in citable form, before publication of the edited article. This *Accepted Manuscript* will be replaced by the edited and formatted *Advance Article* as soon as this is available.

To cite this manuscript please use its permanent Digital Object Identifier (DOI®), which is identical for all formats of publication.

More information about *Accepted Manuscripts* can be found in the **Information for Authors**.

Please note that technical editing may introduce minor changes to the text and/or graphics contained in the manuscript submitted by the author(s) which may alter content, and that the standard **Terms & Conditions** and the **ethical guidelines** that apply to the journal are still applicable. In no event shall the RSC be held responsible for any errors or omissions in these *Accepted Manuscript* manuscripts or any consequences arising from the use of any information contained in them.

Page 1 of 12

CREATED USING THE RSC REPORT TEMPLATE (VER. 3.1) - SEE WWW.RSC.ORG/ELECTRONICFILES FOR DETAILS

REVIEW

Faraday Discussions

www.rsc.org/xxxxxx | XXXXXXXX

View Article Online

Active and Passive Control of Zinc Phthalocyanine Photodynamics

Divya Sharma[a]*, Annemarie Huijser[a], Janne Savolainen[b], Gerwin Steen[a] and Jennifer L. Herek[a]

In this work we report on the ultrafast photodynamics of the photosensitizer zinc phthalocyanine (ZnPc) and manipulation thereof. Two approaches are followed: active control via pulse shaping and passive control via strategic manipulation in the periphery of the molecular structure. The objective of both of these control experiments is the same: to enhance the yield of the functional pathway and to minimize loss channels. The aim of the active control experiments is to increase the intersystem crossing yield in ZnPc, which is important for application in photodynamic therapy (PDT). Pulse shaping allowed an improvement in triplet to singlet ratio of 15% as compared to a transform-limited pulse. This effect is ascribed to a control mechanism that utilizes multiphoton pathways to higher-lying states from where intersystem crossing is more likely to occur. The passive control experiments are performed on ZnPc derivatives deposited onto TiO_2, serving as a model system of a dye-sensitized solar cell (DSSC). Modification of the anchoring ligand of the molecular structure resulted in an increased rate for electron injection into TiO_2 and slower back electron transfer, improving the DSSC efficiency.

Introduction

Photosensitizers are currently a topic of intense scientific research because of their photophysical properties that hold great promise for application in photodynamic therapy (PDT), blood sterilization, sunlight-activated herbicides and insecticides, biomedical imaging and dye-sensitized solar cells (DSSC).[1] A photosensitizer should have a high absorption cross section at the wavelength suitable for the specific application and excellent photochemical and thermal stabilities. Other important parameters while searching for or designing new photosensitizers involve solubility and tendency to aggregate.
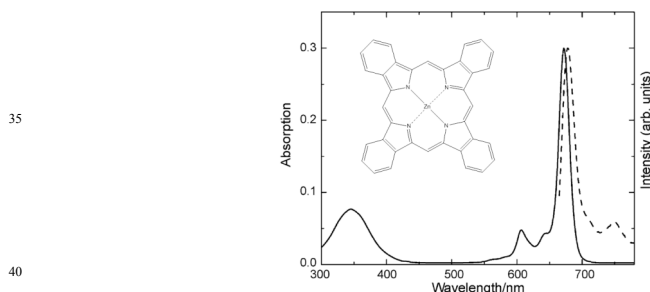

Figure 1. Absorption and fluorescence spectra of ZnPc in DMSO. The inset shows the molecular structure of ZnPc.

Amongst the most promising photosensitizers are zinc phthalocyanines (ZnPcs), planar aromatic molecules with considerable electron delocalization, accounting for unique optical properties. The absorption spectrum of ZnPc in dimethyl sulfoxide

5 (DMSO) is shown in Figure 1. The Q-band $(S_0 \rightarrow S_1)$ has a maximum at 672 nm, as well as vibrational progression to the blue side with a shoulder at 645 nm and a weak band at 606 nm. Further in the ultraviolet, the Soret band $(S_0 \rightarrow S_2)$ with a maximum at 345 nm can be seen. Also included in Figure 1 is the fluorescence spectrum. The fluorescence has a maximum at 680 nm, implying a Stokes shift of 8

10 nm.
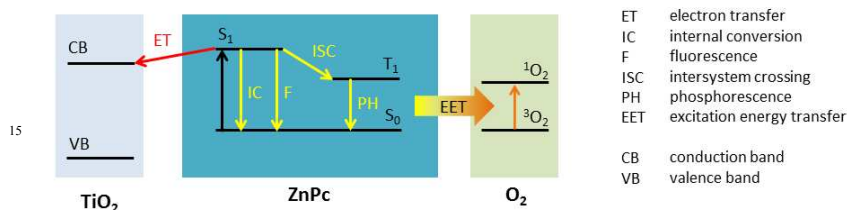
20 Figure 2. Jablonski diagram of the photophysical decay pathways in ZnPc (yellow), ZnPc combined with O_2 (yellow and orange, relevant in PDT) and ZnPc combined with an electron acceptor such as TiO_2 (yellow and red, relevant in DSSC).

PDT is based on three key components: a photosensitizer, a light source and tissue

25 oxygen. The photosensitizer should ideally absorb in the red and near-infrared since human tissue is most transparent in this spectral region. Amongst the most promising photosensitizers for PDT are the phthalocyanines.[1a] The photophysical decay pathways of ZnPc have been studied in detail earlier and are summarized in Figure 2.[2] Absorption of a photon leads to the formation of a singlet excited state.

30 Decay pathways of the singlet excited state involve fluorescence (F), internal conversion (IC) and intersystem crossing (ISC). Only the latter process leads to the formation of the PDT-required triplet excited state. The reason is that excitation energy transfer (EET) from the photosensitizer triplet state towards oxygen leads to the formation of highly reactive singlet oxygen. Singlet oxygen is phototoxic to

35 cancer cells and its presence leads to cell death. A PDT photosensitizer is hence required to have a high ISC yield, which means that the intersystem crossing rate has to be competitive to the unwanted singlet decay channels (F and IC). Manipulation of the photodynamics in favor of ISC is thus essential in the development of efficient PDT photosensitizers.

40 Since the solar emission photon flux has a maximum between 650 nm and 750 nm, phthalocyanines are also considered as promising photosensitizers in DSSCs.[1d] DSSCs are a low-cost alternative to conventional silicon-based solar cells and consist of a semiconductor such as TiO_2 coated with a light-absorbing photosensitizing dye. The photophysical pathways of a DSSC are illustrated in

45 Figure 2 and elaborated in Figure 3A. Absorption of a photon by the dye leads to formation of a strongly bound electron-hole pair (exciton). Efficient exciton dissociation into charge carriers is only possible at the interface between dye and semiconductor and occurs via electron transfer (ET) from the dye into the semiconductor; back electron transfer has to be avoided. Formed charge carriers

50 need subsequently to be transported from the dye-semiconductor interface towards the electrodes. The fact that excitons are usually only able to diffuse over distances of a few nm, while a layer thickness in the order of 100 nm is required for sufficient light-absorption, was the reason for Grätzel and co-workers to introduce the concept of a network of TiO_2 nanoparticles coated with a monolayer of dye molecules and

filled with a liquid I^-/I_3^- electrolyte.[3] The use of ruthenium-based photosensitizer dyes has resulted in efficiencies up to 11% ,[4] though drawbacks involve the price of ruthenium and lack of absorption in the red/near-infrared region of the solar emission spectrum.

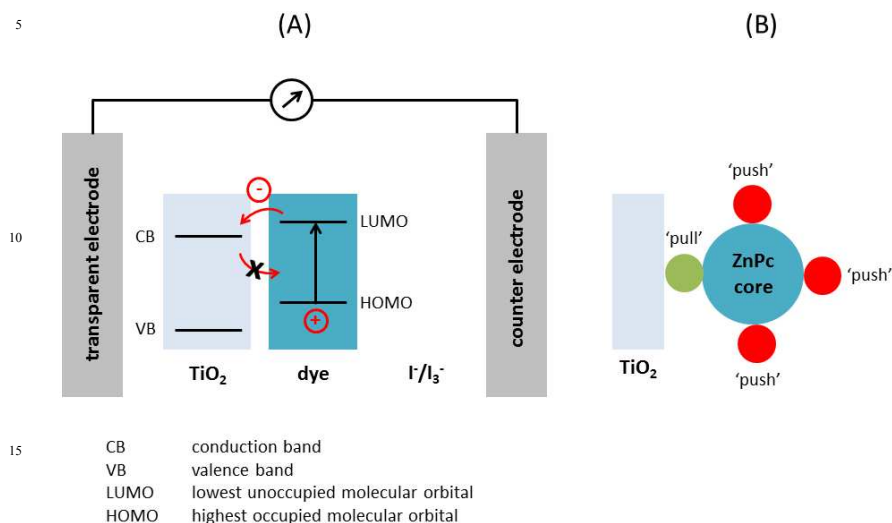| CB | conduction band |
VB	valence band
LUMO	lowest unoccupied molecular orbital
HOMO	highest occupied molecular orbital

Figure 3. Photophysical principles of a dye-sensitized solar cell (DSSC) (A) and an asymmetric push-pull ZnPc photosensitizer with electron transfer directed towards the TiO_2 (B).

Phthalocyanines not only have the ideal absorption spectrum, but are also highly stable chemically and do not contain precious elements. DSSCs based on phthalocyanines, however, have shown poor device efficiencies that did not exceed 1% for a long time.[5] Only recently significantly higher efficiencies up to ~5% have been realized.[6] Important tools in the development towards higher efficiencies involve the prevention of aggregation, by the use of a co-solvent or introduction of bulky side groups, and introducing directionality of the electron transfer process towards the TiO_2. The latter has been realized by replacing a symmetric phthalocyanine by an asymmetric equivalent with one electron pulling group and three electron pushing groups, as visualized in Figure 3B. The electron pushing groups are required to suppress aggregation. Only the electron pulling group should be able to anchor onto the TiO_2 substrate. The observation that adapting the chemical structure from symmetrical into an unsymmetrical push-pull structure leads to a substantial improvement in efficiency suggests a significant change in forward and back electron transfer photodynamics. However, ultrafast photodynamics studies have not been reported so far.

In this work we explore the ultrafast photodynamics of ZnPc and manipulation thereof. Two approaches are followed: active control via pulse shaping and passive control via strategic changes in the periphery of the molecular structure. The aim of these control experiments is to enhance the yield of the functional pathway and minimize loss channels. Actively, this entails illuminating the photosensitizer with an ideally shaped pulse instead of a transform-limited (i.e. unshaped) pulse. We will use this approach to manipulate the ISC yield. The objective of the passive control experiment is to manipulate electron transfer from ZnPc into TiO_2 and the undesirable back electron transfer by adapting the chemical structure of the anchoring electron pulling group.

Results

ZnPc photophysics

A detailed description of the pump-probe setup was reported earlier.[2] ZnPc in
5 DMSO was excited at 672 nm (22 fs, 30 nm FWHM).   Photophysical processes
were monitored in time using a delayed white-light continuum as a probe, which was
generated by sending part of the amplified fundamental 775 nm beam through a
delay line and into a sapphire window. To avoid any anisotropy effects, the
polarization angle between the pump and the probe pulses was set to 54.7°.

10 Figure 4 shows the pump-probe data as a function of time and wavelength of ZnPc
in DMSO. The 2D-surface is a combination of broad excited state absorption (ESA)
bands superimposed with negative signals due to ground state bleach (GSB) and
stimulated emission (SE). The negative band (A) reflects a combined GSB and SE.
The positive bands at early time scales (B1 and B2) is due to ESA of the singlet
15 excited state. Evolution of this state into a triplet excited state via ISC is reflected by
the decay of B1 and B2 and the rise of the triplet ESA band (C).[2] Observation of
branching in the deactivation of the ZnPc singlet excited state indicates the
possibility of performing coherent control experiments to actively enhance the ISC
yield via pulse shaping. In fact, recent 2D electronic spectroscopy reveals
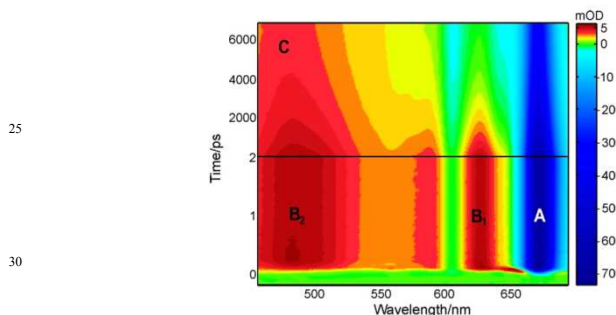20 coherences in the excited state dynamics.[7]

Figure 4. Pump-probe data as function of time and wavelength of ZnPc in DMSO.
35 The characteristic features of stimulated emission and bleach (A), singlet ESA (B1
and B2) and triplet ESA (C) are indicated. Note the two different time windows and
non-linear intensity scaling, used to emphasize the ultrafast dynamics.

Active control

Coherent control is a spectroscopic tool that can drive and control the temporal
40 evolution of a system to a desired product channel by optimally shaping the time-
dependent electric field of the laser pulse and has been used to control isomerization
reactions, excitation energy transfer in natural and artificial light-harvesting
complexes, selective excitation of vibrational modes and population transfer.[8] The
phases and/or amplitudes of different frequency components of the laser pulse are
45 matched to the inherent molecular resonances and dynamics to selectively address
and steer them to the target state. Thus, coherent control provides a powerful means
for manipulation on the molecular scale, facilitated by active tuning of laser pulse
parameters such as frequency, phase, amplitude, and polarization. Here, the aim of
the optimization experiment is to find an optimum laser shape that improves the ISC
50 yield and as a consequence the efficiency of ZnPc in generating singlet oxygen.

Since for a polyatomic molecule such as ZnPc the complete Hamiltonian is too

complex to determine the driving optical field in advance, an iterative closed-loop feedback optimization[9] was performed. The sample was excited using shaped femtosecond pulses (~672 nm) with a pulse energy of 500 nJ/pulse. The learning loop consists of a pulse shaper, the ZnPc sample and an evolutionary learning
5 algorithm. The evolutionary algorithm was started with a set of random phases; the resulting pulse shapes were tested on the sample. The feedback signal obtained from the transient absorption experiment was evaluated via a fitness function, from which a new set of pulse shapes were generated and applied. The feedback signal for the singlet (S) state was obtained by integrating a 10 nm band from the transient
10 spectrum at 20 ps time delay at the maximum of the ESA band (centered at 490 nm). The feedback signal for the triplet (T) state was measured at 25 ns time delay at the maximum of the triplet ESA at 480 nm with a bandwidth of 15 nm. The fitness functions were $f = T/S$ and $f = S/T$, respectively. The evolutionary algorithm iteratively optimized the value of the feedback function (i.e. T/S and S/T) relative to
15 that of a transform-limited (TL) pulse. The shape of the optimized pulse was characterized by using a frequency-resolved cross-correlation measurement (X-FROG). Figure 5 shows the obtained learning curves for T/S and S/T and fitness of the TL pulse measured before each generation. Obviously it is possible to increase the T/S ratio by a factor of ~1.15 and the S/T ratio by a factor of ~1.05. The X-
20 FROG traces of the best pulses for both cases show complicated structures that are difficult to interpret directly.
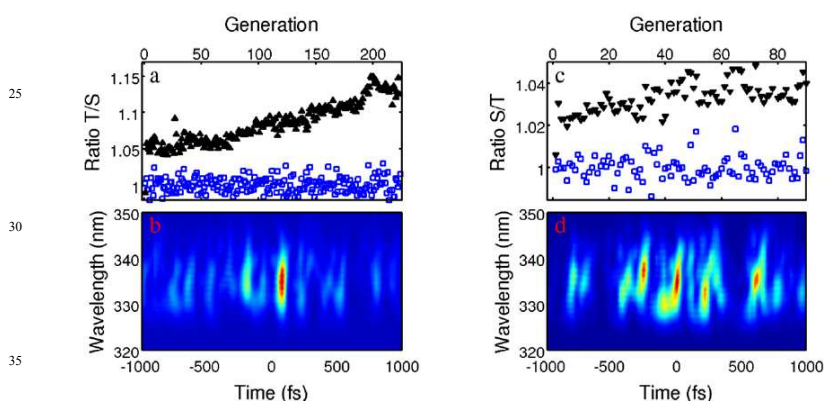

Figure 5. Optimal control results on the triplet yield of ZnPc. Panel a: The obtained learning curve (black) for the ratio T/S and fitness of the TL pulse measured before
40 each generation (blue). Panel b: The X-FROG surface of the best pulse. Panel c: The obtained learning curve (black) for the ratio S/T and fitness of the TL pulse measured before each generation (blue). Panel d: The X-FROG surface of the best pulse.

To verify the robustness and to further understand the obtained optimal control
45 results, repeated measurements were done where the fitnesses of the found best pulse shapes were remeasured. Figure 6a shows the repeated optimization; the T/S ratio is improved by a factor of ~1.10. Also included is the so-called actinic energy of the best individual pulses along the optimization. Actinic energy is simply an integrated sum of the pump spectrum, amplitude mask and the absorption spectrum
50 of the ZnPc. The shown values are normalized to 100% for the flat amplitude mask with no amplitude shaping. The actinic energy first drops to ~47% of the initial value, which is expected for the random amplitude mask of the first generation. Thereafter, the actinic energy stays fairly constant varying ~13%. It is interesting to compare the relation between the actinic energy and the obtained fitnesses. The
55 initial fall of ~53% in the actinic energy results in an increase of the T/S ratio of

~6%. However, later, along the optimization such correlations cannot be found. For instance, while from generation 50 to 100 the T/S ratio rises with the slightly increasing actinic energy, from generation 150 to 200 the opposite holds: increasing fitness with decreasing actinic energy. Figure 6b shows the behaviour of the
5 individual signals belonging to T and S during the repeated measurement shown in Fig. 6a. The overall population transfer decreases as both of the channels show decreasing signals. However, it is evident that the difference between the two signals shows a jump with the initial fall of the actinic energy and then slowly expands along the learning curve. In conclusion, the data show that the control involves other
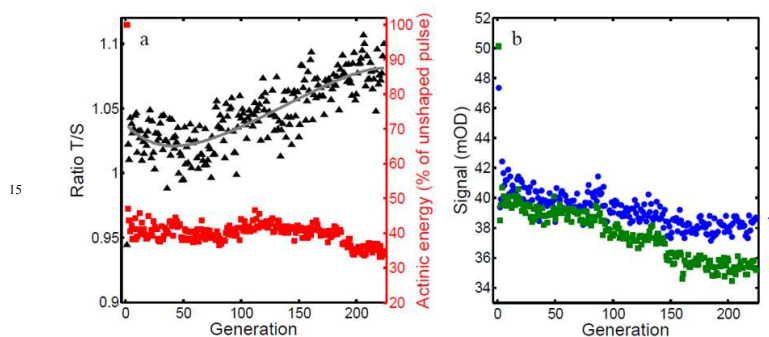10 features than trivial solutions related to the pulse intensity.

20 Figure 6. Repeated measurement of the T/S optimization. Panel a: The ratio T/S (black) and normalized actinic energy (red). The grey line is a polynomial fit to guide the eye. Panel b: The triplet signal (blue circles) and the singlet signal (green squares).

To further investigate the importance of the pulse intensity to the control, we
25 conducted intensity dependence measurements using a TL pulse with varying intensities. Figure 7 shows S and T signals as a function of pump intensity. A difference in the shape of the saturation curves of S and T is reflected in the fitness value as an increase of the ratio T/S with decreasing pump intensity. This is in good agreement with what was observed in the T/S optimal control experiments: an initial
30 drop in the pump intensity to some 47% of the initial energy of 500 nJ/pulse results in a step-wise increase of the fitness value in the beginning of the optimization.
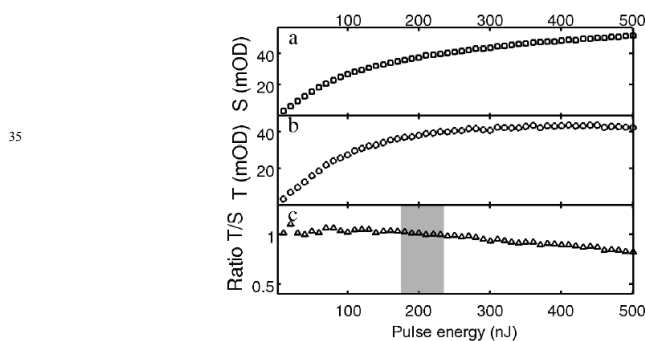

Figure 7. Intensity dependence of the feedback signals using a TL pulse. Singlet and triplet states show slightly different behaviour resulting in a decreasing ratio T/S with pulse intensity. The grey area indicates the actinic energy regime used by the
45 algorithm in the course of the optimization.

However, quantitatively the jump from 500 to 235 nJ/pulse with TL pulse causes a larger (~17%) jump in the fitness compared to the one observed in the optimization and the repeated measurement (~6%, see Figure 6). Further, as is shown in Figure 7, the fitness variation of the TL pulse in the actinic energy range of the optimization is
5 less than 4% and therefore cannot be behind the learning process. This indicates that the actual shape of the pulse bears importance implying the involvement of more complicated mechanisms than signal saturation.

Open-loop phase scans were performed using the amount of linear chirp and the spectral location of π phase steps as variables. Figure 8a shows the T and S signal
10 and their ratio (T/S) as a function of the applied linear chirp. Both S and T decrease similarly on introducing more negative chirp. Positive chirp leads to a different behaviour: S remains constant whereas T grows gradually. This variation can be seen in the asymmetric shape of the ratio T/S. The overall shape of the chirp scan traces points to a pump-dump mechanism that reduces the population on the excited
15 state demonstrated previously in a study on the fluorescence emission yield of the green fluorescent protein (GFP).[10] As the initially excited wavepacket slides down the potential energy surface of the first excited state, a negatively chirped pulse can dump it back to the ground state whereas a positively chirped pulse is not able to produce such an effect. However, this well established mechanism does not explain
20 the different behaviour of the two channels, i.e. the gradual growth that was observed for the T trace. Therefore, chirp scans as a function of the pulse intensity were also done (data not shown). Unlike in the GFP study,[10] overall features remained similar (reduced S and T with negative chirp), but the difference between T and S vanished with reduced intensity. This could be an indication of a
25 multiphoton process involving higher-lying excited states. The evolution of the wavepacket on the potential energy surface of the first excited state can vary the transition probabilities of possible sequential two photon absorption processes. By following this evolution a chirped pulse can enhance the yield of such processes, which then leads to more efficient triplet formation.
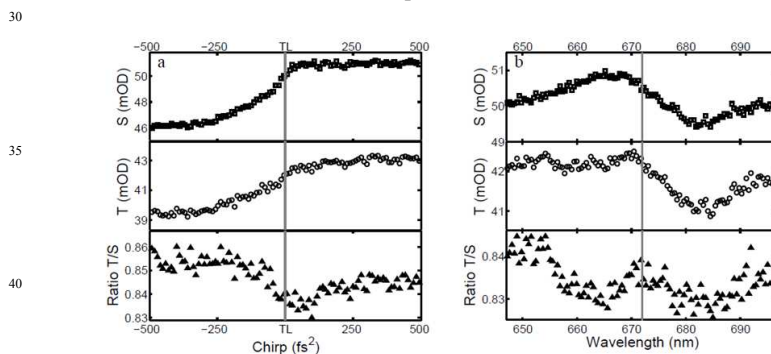

Figure 8. Open-loop control results. Panel a: Chirp scan, the feedback signals S, T
45 and the T/S ratio when a linear chirp is scanned from negative to positive. The grey line indicates a TL pulse. Panel b: π-phase jump scan where the feedback signals S, T and the T/S ratio are measured when the spectral position of a step function having a π phase jump is scanned over the pump spectrum. The grey line indicates the peak of the resonance.

To further test the involvement of multiphoton processes, π-phase-jump scanning where the spectral position of a step function with an amplitude of π is scanned over the pump spectrum while recording the feedback signals, was used. The results in Figure 8b shows that the T and S signals are dependent on the location of the phase
55 jump. The overall shape of the S and T traces resembles the imaginary part of resonance that describes absorption. The phase profile of the pulse modulates the

population transfer by compensating the natural phase flip occurring at resonance. Furthermore, the ratio T/S has a different shape having a maximum at the peak of the absorption band at 672 nm, and U-shaped features symmetrically around it. The T/S ratio trace bears a striking resemblance to previous results on multiphoton transitions.[11] The T/S trace is an intermediate example between a narrow atomic transition and a broad molecular transition of a multiphoton control curve. Qualitatively this makes sense as the width of the ZnPc absorption band is between the widths of Cesium and Coumarin 6H used in reference.[11] In conclusion, the π-phase jump scan supports the hypothesis that multiphoton processes are involved in the control mechanism. It has previously been shown that unlike in the case of nonresonant two-photon absorption TL pulses are not optimal for two-photon transitions involving an intermediate resonant state.[12] Considering this together with the results from the chirp and π-jump scans, we propose a control mechanism that utilizes multiphoton pathways to higher-lying states from where ISC is more probable, thus leading to the enhancement of the triplet yield. A similar mechanism has also been proposed in a previous study on the triplet yield in β-carotene by Buckup et al.[13]

Passive control

Two asymmetric push-pull zinc phthalocyanine DSSC photosensitizers were studied, namely TT1 and TT7; the molecular structures are shown in Figure 9.
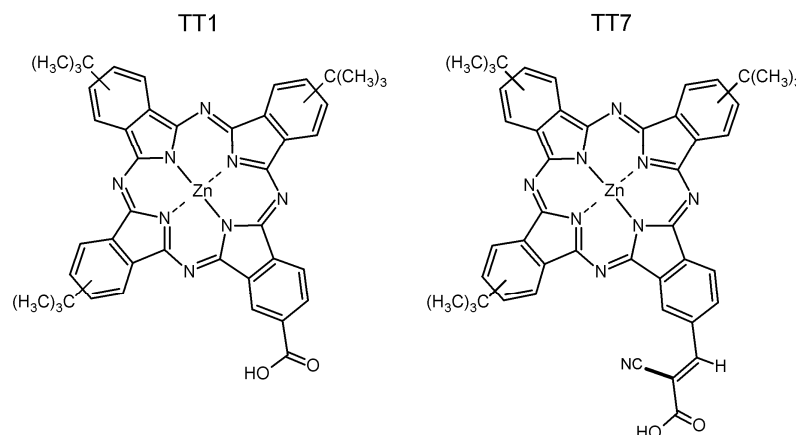

Figure 9. Molecular structures of zinc phthalocyanine derivatives TT1 and TT7.

The synthesis of TT1 and TT7 was reported in detail earlier.[14] TT1 is an asymmetric zinc phthalocyanine with one electron pulling and anchoring carboxylic acid group, and three *tert*-butyl groups with electron pushing and aggregation suppressing character. TT7 has similar *tert*-butyl groups, however the anchoring group differs substantially. The carboxylic acid group is no longer in direct contact with the phthalocyanine core, but connected via a conjugated bridge. The conjugated bridge in TT7 is equipped with an electronegative CN group promoting directionality of the ET process in the direction of the TiO_2. The modification of the anchoring group can be expected to change both the forward ET from the phthalocyanine into the TiO_2 as well as the unwanted back ET process. The increased distance between the phthalocyanine core and the TiO_2 is expected to slow down both processes. Due to its electronegative character, the CN group might increase the rate of the ET processes. The observation that DSSCs based on the two derivatives show a

Faraday Discussions

substantial difference in efficiency (2.55% for TT7 and 3.56% for TT1[14]) suggests a significant effect on the interface dynamics.

Colloidal TiO_2 paste (Ti-Nanoxide HT) was purchased from Solaronix. The particle size is specified to be 8-10 nm and the paste is well-suited for the preparation of
5 transparent electrodes for DSSC. The TiO_2 paste was spread onto a glass sheet using tape as a spacer. A thin film was obtained by raking off the excess of paste with a glass rod. After removing the tape and drying in air, the sample was sintered in air at 450 °C for 30 min. The obtained transparent TiO_2 coated glass substrate was dipped for 4 hours into a 0.1 mM solution of the zinc phthalocyanine derivative in ethanol
10 containing 20 mM 3a,7a-dihydroxy-5b-cholanic acid (Cheno, purchased from Sigma Aldrich) and finally rinsed several times with ethanol.

The absorption spectra of the ZnPc derivatives in solution and deposited onto TiO_2 are shown in Figures 10A and 10B. The Q-band observed for TT1 sensitized TiO_2 at 685 nm is due to monomers and the band at 635 nm is partly due to a vibrational
15 progression of the monomer absorption and due to the presence of aggregates. The corresponding bands for TT7 sensitized TiO_2 are at 645 nm and a shoulder at 690 nm. The absorption spectra of both the TT1 and TT7 sensitized TiO_2 substrates are broadened as compared to those in solutions (Figure 10A), which can be attributed to an increased inhomogeneity of the molecular environment. The fluorescence
20 spectra of TT7 in solution exhibits a ~14 nm red shift (peak at 704 nm) as compared to that of TT1 in solution (peak at 690 nm) (see Figure 10C). The fluorescence of the sensitized TiO_2 substrates was observed to be heavily quenched (data not shown).

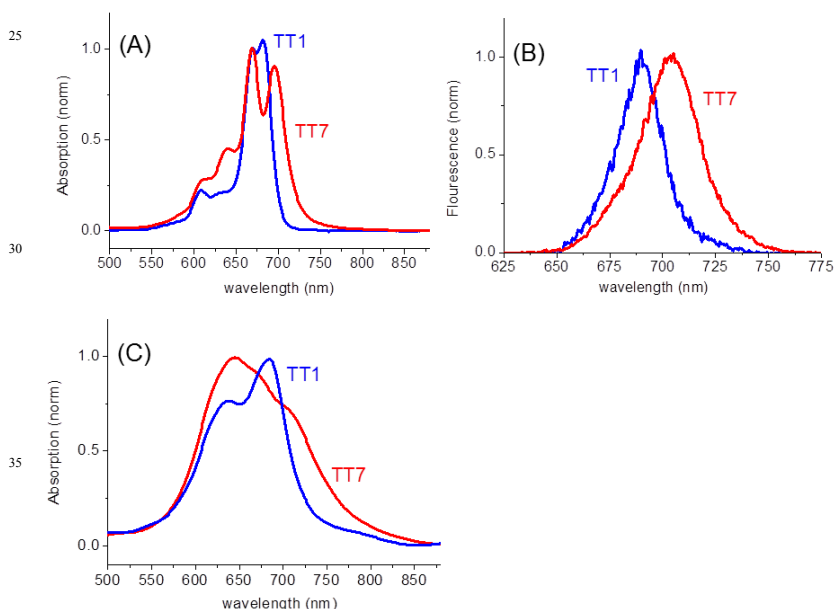40 Figure 10. Absorption (A) and fluorescence spectra (B) of TT1 and TT7 in solution (1×10^{-4} M in ethanol containing 20 mM Cheno) and the absorption spectra (C) of TT1 and TT7 sensitized TiO_2 substrates.

Pump-probe data were recorded upon excitation at 680 nm (80 fs, 40 nm FWHM) to minimize the contribution of aggregates to the dynamics. Pump pulses with an energy of 20 nJ/pulse were focused to a spot-size of 130 μm which correspond to a photon flux of 5×10^{14} photons/cm^2 and was verified to be in the linear regime. Transient dynamics were probed by using a white light continuum (470 nm-700 nm) generated by focusing a part of the fundamental (775 nm) into a 2 mm sapphire window. The relative polarization of pump and probe was kept at 54.7°. The photosensitized TiO$_2$ substrate was mounted on an automated mechanical translational stage to avoid photodegradation.

Electron injection from a photosensitizer into TiO$_2$ is known to occur with various rate constants, typically an ultrafast component ~100 fs followed by a slower ps component. This is explained in terms of a two-state relaxation model, the fast component is attributed to electron injection from the nonthermalized state whereas the ps component is due to electron injection from the relaxed excited state. This difference in electron injection time arises from a variation of the density of states in the TiO$_2$ for different energy levels. The biphasic behavior is known to be particularly pronounced for Ru polypyridyl complexes on TiO$_2$ and applies to lower extent to organic chromophores.[15] Literature values for zinc phthalocyanine derivatives deposited on TiO$_2$ are 296 fs [16] and <500 fs.[5b] For a zinc porphyrin derivative a value of 300 fs was reported.[17] Back electron transfer times cover a wide range from the ps till the ms domain, important factors are the absence/presence of an electrolyte, electrodes and bias voltage.[18] Geminate recombination, i.e. back electron transfer to its origin, typically occurs in the ps domain, while back transfer of delocalized electrons is known to be slower.[17]
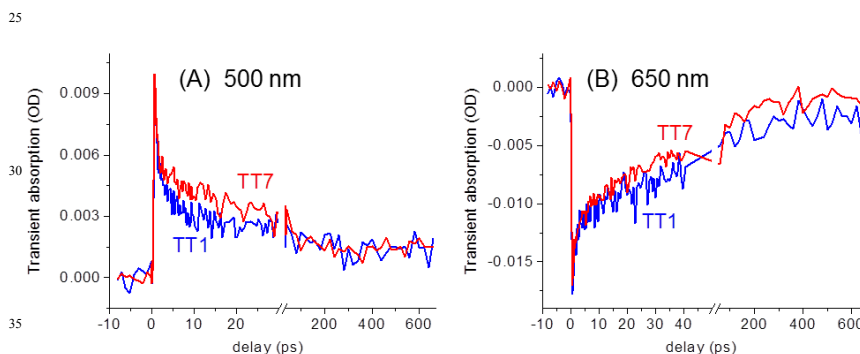

Figure 11. Transient absorption kinetics of TT1 and TT7 sensitized nanocrystalline TiO$_2$ at 500 nm (A, representing ESA) and 650 nm (B, representing GSR).

Figure 11A shows the transient absorption kinetics of TT1 and TT7 sensitized TiO$_2$ substrates at 500 nm, where the signal is predominantly due to singlet ESA. Both samples show an initial ultrafast decay ~500 fs, followed by a slower ps decay component, which is much faster than the ESA decay observed for the ZnPc in solution (Figure 4). The ps component is considerably faster for TT1 (~4 ps) than for TT7 (~15 ps), indicating faster electron injection. The transient spectral evolution shows the development of a positive band around 560 nm, which can be attributed to the oxidized photosensitizer. [6b,19] This band appears within 1 ps, consistent with the ultrafast decay of the ESA and again reflecting electron injection into the TiO$_2$.

A signature of back electron transfer from the TiO$_2$ to the photosensitizer involves the ground state recovery (GSR). GSR is probed at 650 nm, at which wavelength stimulated emission is marginal (see also Figure 10C). Figure 11B shows the GSR kinetics of TT1 and TT7 sensitized TiO$_2$ substrates. Recombination occurs at time

scales of 1-2 ps and tens of ps (TT1: 60 ps, TT7: 50 ps) and is slightly faster for TT7 than for TT1.

In summary, strategic manipulation in the periphery of the molecular structure allows passive control of the interface dynamics. The TT1 sensitized TiO_2 substrate shows faster injection and slower recombination as compared to TT7, explaining the lower efficiency observed for a DSSC based on the latter photosensitizer.[14] Apparently the effect of the increased distance between the phthalocyanine core and the TiO_2 for TT7 is greater than the impact of the electronegative CN group resulting in a slower electron injection. The presence of the electron pulling CN group might however promote the back electron transfer from the TiO_2 to the photosensitizer leading to faster recombination.

Conclusions

In this work we report on the manipulation of the ultrafast photodynamics of the photosensitizer zinc phthalocyanine (ZnPc) via active and passive control. Pulse shaping allowed an improvement in triplet to singlet ratio of 15% as compared to exposure to a transform-limited pulse. This effect is ascribed to a control mechanism that utilizes multiphoton pathways to higher-lying states from where intersystem crossing is more likely to occur. Manipulation of the periphery of the molecular structure resulted in an increased rate for electron injection into TiO_2 and slower back electron transfer, improving the DSSC efficiency.

Acknowledgments

References

ª Optical Sciences group, MESA+ Institute for Nanotechnology, University of Twente, PO Box 217, 7500 AE, Enschede, The Netherlands. Fax: +31 53 489 3511; Tel: +31 53 489 3805. E-mail: d.sharma@utwente.nl.

ᵇ Physikalisch-Chemisches Institut, Universität Zürich, Winterthurerstrasse 190, CH-8057 Zürich, Switzerland.

1   M. C. DeRosa and R. J. Crutchley, *Coordin Chem Rev*, 2002, **233**, 351; M. Ochsner, *J Photoch Photobio B*, 1997, **39**, 1; M. V. Martinez-Diaz, G. de la Torrea and T. Torres, *Chem Commun*, 2010, **46**, 7090; M. V. Martinez-Diaz, M. Ince and T. Torres, *Monatsh Chem*, 2011, **142**, 699.

2   J. Savolainen, D. van der Linden, N. Dijkhuizen and J. L. Herek, *J Photoch Photobio A*, 2008, **196**, 99.

3   B. Oregan and M. Gratzel, *Nature*, 1991, **353**, 737.

4   M. Gratzel, *J Photoch Photobio A*, 2004, **164**, 3.

5   M. K. Nazeeruddin, R. Humphry-Baker, M. Gratzel, D. Wohrle, G. Schnurpfeil, G. Schneider, A. Hirth and N. Trombach, *J Porphyr Phthalocya*, 1999, **3**, 230; J. J. He, G. Benko, F. Korodi, T. Polivka, R. Lomoth, B. Akermark, L. C. Sun, A. Hagfeldt and V. Sundstrom, *J Am Chem Soc*, 2002, **124**, 4922.

6   P. Y. Reddy, L. Giribabu, C. Lyness, H. J. Snaith, C. Vijaykumar, M. Chandrasekharam, M. Lakshmikantam, J. H. Yum, K. Kalyanasundaram, M. Graetzel and M. K. Nazeeruddin, *Angew Chem Int Edit*, 2007, **46**, 373; J. J. Cid, M. Garcia-Iglesias, J. H. Yum, A. Forneli, J. Albero, E. Martinez-Ferrero, P. Vazquez, M. Gratzel, M. K. Nazeeruddin, E. Palomares, T. Torres, *Chem-Eur J*, 2009, **15**, 5130; M. E. Ragoussi, J. J. Cid, J. H. Yum, G. de la Torre, D. Di Censo, M. Gratzel, M. K. Nazeeruddin and T. Torres, *Angew Chem Int Edit*, 2012, **51**, 4375; S. Mori, M. Nagata, Y. Nakahata, K. Yasuta, R. Goto, M. Kimura and M. Taya, *J Am Chem Soc*, 2010, **132**, 4054.

7   T. Mančal, N. Christensson, V. Lukeš, F. Milota, O. Bixner, H. F. Kauffmann and J. Hauer, *Phys Chem Lett*, 2012, **3**, 1497.

8   Y. Silberberg, *Annu Rev Phys Chem*, 2009, **60**, 277.

9   J. Savolainen, R. Fanciulli, N. Dijkhuizen, A. L. Moore, J. Hauer, T. Buckup, M. Motzkus and J. L. Herek, *P Natl Acad Sci USA*, 2008, **105**, 7641.

10   C. J. Bardeen, V. V. Yakovlev, J.A. Squier, K. R. Wilson, *J Am Chem Soc*, 1998, **120**, 13023.

11   D. Meshulach and Y. Silberberg, *Phys Rev A*, 1999, **60**, 1287.

12   N. Dudovich, B. Dayan, S. M. G. Faeder and Y. Silberberg, *Phys Rev Lett*, 2001, **86**, 47.

13   T. Buckup, T. Lebold, A. Weigel, W. Wohlleben and M. Motzkus, *J Photoch Photobio A*, 2006, **180**, 314.

14   M. Garcia-Iglesias, J. J. Cid, J. H. Yum, A. Forneli, P. Vazquez, M. K. Nazeeruddin, E. Palomares, M. Gratzel and T. Torres, *Energ Environ Sci*, 2011, **4**, 189.

15   N. A. Anderson and T. Q. Lian, *Annu Rev Phys Chem*, 2005, **56**, 491.

16   D. Ino, K. Watanabe, N. Takagi and Y. Matsumoto, *J Phys Chem B*, 2005, **109**, 18018.

17   C. W. Chang, L. Y. Luo, C. K. Chou, C. F. Lo, C. Y. Lin, C. S. Hung, Y. P. Lee and E. W. G. Diau, *J Phys Chem C*, 2009, **113**, 11524.

18   S. A. Haque, Y. Tachibana, R. L. Willis, J. E. Moser, M. Gratzel, D. R. Klug and J. R. Durrant, *J Phys Chem B*, 2000, **104**, 538.

19   P. Charlesworth, T. G. Truscott, R. C. Brooks and B. C. Wilson, *J Photoch Photobio B*, 1994, **26**, 277.